CHEMISTRY OF MATERIALS

pubs.acs.org/cm

Article

Direct Band Gap Chalcohalide Semiconductors: Quaternary $AgBiSCl_2$ Nanocrystals

Danila Quarta,[†] Stefano Toso,[†] Antonio Fieramosca, Lorenzo Dominici, Rocco Caliandro, Anna Moliterni,* David Maria Tobaldi, Gabriele Saleh, Irina Gushchina, Rosaria Brescia, Mirko Prato, Ivan Infante, Adriano Cola, Cinzia Giannini, Liberato Manna, Giuseppe Gigli, and Carlo Giansante*

Cite This: *Chem. Mater.* 2023, 35, 9900−9906

Read Online

ACCESS | Metrics & More | Article Recommendations | Supporting Information

ABSTRACT: Heavy pnictogen chalcohalide semiconductors are coming under the spotlight for energy conversion applications. Here we present the colloidal synthesis of phase pure $AgBiSCl_2$ nanocrystals. This quaternary chalcohalide compound features a quasi-two-dimensional crystal structure and a direct band gap, in contrast with the monodimensional structure and the indirect band gap peculiar to the orthorhombic, ternary Bi chalcohalides. Consistently, colloidal $AgBiSCl_2$ nanocrystals exhibit photoinduced luminescence compatible with both band edge excitons and midgap states. This is the first observation of band edge emission in chalcohalide nanomaterials at large, although exciton recombination in our $AgBiSCl_2$ nanocrystals mostly occurs via nonradiative pathways. This work further advances our knowledge on this class of mixed anion semiconductor nanomaterials and provides a contribution to establishing chalcohalides as a reliable alternative to metal chalcogenides and halides.

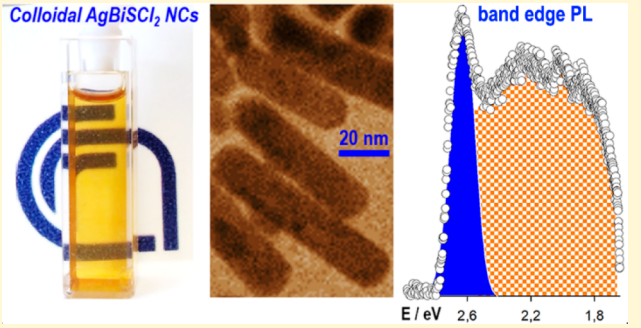

INTRODUCTION

Heavy pnictogen chalcohalides are semiconductor materials considered as promising candidates for energy conversion purposes, including photovoltaic and thermoelectric devices, photo(electro)catalysts, and piezoelectric generators, among others.[1,2] Heavy pnictogen chalcohalides have good chemical stability combined with tunable band gaps and high absorption coefficients, and additionally, they are constituted by low-toxicity elements.[3,4] The control over the size distribution of chalcohalide crystals and their processability is a further criterion for the development of chalcohalide-based devices, which we recently addressed by proposing a synthetic method to prepare colloidal dispersions of bismuth chalcohalide nanocrystals (NCs) with a rather low polydispersion.[5,6] Colloidal NCs of orthorhombic BiEX (with E = S, Se and X = Cl, Br, I)[5] and hexagonal $Bi_{13}S_{18}X_2$ (with X = Br, I)[6] phases have high absorption coefficients (up to above 10^5 cm^{-1}) and tunable band gaps spanning the visible and near-infrared spectral region (from 2.1 to 0.80 eV). However, the lowest energy interband transition is indirect in all of these compounds. Although an indirect band gap is not necessarily a drawback for effective light harvesting,[7] it is a limitation for light emission. Therefore, the quest for direct band gap chalcohalides holds both fundamental and practical importance, as few compounds in this class are known as direct semiconductors. As an example, a direct band gap was reported for some quaternary chalcohalides,[8] including $Pb_2BiS_2I_3$ that was also recently prepared via a solution-phase method.[9] However, the demand for semiconductors containing low-toxicity elements would suggest to focus on Sn analogues (such as $Sn_2BiS_2I_3$).[8] Another chalcohalide compound that might fulfill these requirements is $AgBiSCl_2$,[10−12] for which solution-phase synthetic methods are lacking so far.

Here, we extend our method for the preparation of heavy pnictogen chalcohalide NCs[5,6] to the synthesis of colloidal NCs of the $AgBiSCl_2$ phase. We ascertained, by structural data obtained with synchrotron light, the phase purity and the preferential growth direction of our NCs; moreover, we computationally assessed the direct character of the band gap of $AgBiSCl_2$ and experimentally observed the photoinduced luminescence (PL) of our NCs. The PL likely stems from both band edge and intragap (trap) states, although nonradiative paths dominate exciton recombination.

EXPERIMENTAL SECTION

Chemicals. All chemicals were of the highest purity available unless otherwise noted and were used as received. Bismuth(III)

Received: June 6, 2023
Revised: November 7, 2023
Accepted: November 7, 2023
Published: November 27, 2023

acetate ($Bi(Ac)_3$; 99.99%) was purchased from Alfa Aesar. Silver(I) acetate (AgAc; 99.9%), oleic acid (OlCOOH, technical grade, 90%), dodecanethiol (DoSH, 98%), 1-octadecene (technical grade, 90%), and bis(trimethylsilyl)sulfide ($(Me_3Si)_2S$; synthesis grade) were purchased from Sigma-Aldrich. Benzoyl bromide (BzBr; 97%) was purchased from Acros Organics. Benzoyl chloride (BzCl; ≥98%) was purchased from TCI Europe. All solvents were anhydrous and used as received. Tetrachloroethylene was purchased from Merck; toluene and acetone were purchased from Sigma-Aldrich.

Synthesis. The colloidal chalcohalide NCs were synthesized in three-neck flasks connected to a standard Schlenk line under oxygen- and moisture-free conditions. In a typical synthesis yielding colloidal NCs of the $AgBiSCl_2$ phase, the metal precursor solutions were prepared separately and then mixed. The Bi precursor was prepared as following: 0.15 mmol (60 mg) of $Bi(Ac)_3$ and ten equivalents (1.5 mmol; 430 mg) of OlCOOH were mixed in 1.5 g of 1-octadecene; the mixture was vigorously stirred and deaerated through repeated cycles of vacuum application and purging with nitrogen at about 80 °C; the mixture was then heated to above 100 °C to dissolve $Bi(Ac)_3$ until the solution became colorless and optically transparent, suggesting the complete formation of the bismuth(III)-oleate complex(es). The Ag precursor was prepared as follows: 0.15 mmol (25 mg) of AgAc and one equivalent (0.15 mmol; 36 μL) of DoSH were mixed in 1.5 g of 1-octadecene; the mixture was vigorously stirred and deaerated through repeated cycles of vacuum application and purging with nitrogen at about 80 °C; the mixture was then heated to above 100 °C to dissolve AgAc until the solution became yellow and optically transparent, suggesting the formation of the silver(I)−thiolate complex(es); attempts of dissolving AgAc in 1-octadecene with (excess) OlCOOH yielded opaque dispersions, suggesting a poor solubility for the resulting Ag−carboxylate complex(es). The Bi-complex solution was then added to the Ag-complex solution, heated at 80 °C and repeatedly subjected to vacuum in an attempt to remove the acetic acid eventually released upon the formation of the metal complexes. The solution was then heated at 130 °C under a nitrogen flow. Once the temperature stabilized, one equivalent of $(Me_3Si)_2S$ (0.15 mmol; 32 μL) and an excess of BzCl (0.50 mmol; 58 μL) were dissolved in 2 mL of octadecene in a nitrogen-filled glovebox and then transferred under the fume hood and swiftly coinjected in the reaction flask. The reaction was allowed to proceed for 150 min; then the heating mantle was removed, and the resulting colloidal dispersion was allowed to cool to room temperature. After the synthesis, the crude product was centrifuged with acetone as an antisolvent and then transferred to a nitrogen-filled glovebox. The supernatant was discarded, and the resulting pellet was redispersed in anhydrous toluene, reprecipitated with acetone, and centrifuged again. The pellet was redispersed in toluene and stored in the glovebox for further use. Any attempt to prepare quaternary sulfobromide NCs was carried out by adapting the former synthetic procedure and using BzBr instead of BzCl.

Caution! $(Me_3Si)_2S$ is vile-smelling and quickly hydrolyzes releasing toxic H_2S: handle in glovebox and use under fume hood; pour remnant solutions into bleach to reduce stench by oxidation; leave glassware in a bleach bath before washing (or disposal).

Morphological Characterization. Bright-field transmission electron microscopy (BF-TEM) imaging was used to obtain information about the NC morphology from dried colloidal dispersions. Conventional TEM images were recorded with a JEOL JEM 1400 Plus microscope, operating at an accelerating voltage of 120 kV. Samples for analysis were prepared by dropping from a NC dispersion onto Cu grids with a carbon support film and then allowing the solvent to evaporate in a vapor controlled environment. Longitudinal and lateral sizes were determined by the statistical analysis of BF-TEM images of several hundreds of NCs with ImageJ software.

Further high-resolution TEM (HR-TEM) imaging, high-angle annular dark field-scanning TEM (HAADF-STEM) imaging, and elemental mapping were carried out using a Thermo Fisher Scientific Tecnai F20, operated at 200 kV, equipped with an X-Flash 6T|30 silicon-drift detector (SDD) for energy-dispersive X-ray spectroscopy (EDS). For these analyses, the samples were drop-cast onto a holey carbon film on a Cu grid.

Compositional Characterization. X-ray photoelectron spectroscopy (XPS) was used to determine the elemental composition of the NCs. XPS spectra were recorded with a Kratos Axis Ultra^{DLD} spectrometer, using a monochromatic Al Kα source operated at 20 mA and 15 kV. Wide scan analyses were carried out with an analysis area of 300 × 700 μm and a pass energy of 160 eV. High-resolution analyses on the energy ranges typical for Ag 3d, Bi 4f, S 2p, and Cl 2p signals were carried out with the same analysis area and a pass energy of 10 eV.

Structural Characterization. X-Ray diffraction (XRD) was used to probe the crystal structure of the NCs. Powder XRD (XPD) patterns were acquired on a lab-grade Malvern PANalytical PW 3050/65 X' Pert PRO MRD diffractometer, equipped with a fast RTMS detector, using CuKα radiation (40 kV and 40 mA). Data were collected in the 5−85 °2θ range, with a virtual step-scan of 0.02° 2θ and virtual time-per-step of 200 s. Samples for the analysis were prepared by precipitating the NCs with ethyl acetate, discarding the supernatant, and drying the precipitate under a nitrogen flux. The resulting powder was ground in a mortar to minimize preferential orientation effects and then deposited on a zero-diffraction silicon sample holder for the analysis.

Synchrotron light was used for structural characterization of the colloidal NCs. The X-ray data were collected at the 28ID-2 beamline of the National Synchrotron Light Source (NSLS-II) at Brookhaven National Laboratory. The beamline is equipped by a Perkin-Elmer XRD 1621 digital imaging detector having 2048 × 2048 pixels with 200 × 200 μm pixel size. The $AgBiSCl_2$ NC powder sample was put in a capillary of 1 mm diameter that was spun during data collection to avoid preferred orientation effects. Measurements were performed with a beam energy of 67.16 keV (0.1846 Å) and the detector mounted in two positions suitable for pair distribution function (PDF) and XPD data collections, i.e., respectively 215 and 1384 mm downstream from the samples. Nickel was the standard material measured to calibrate the wavelength and detector geometry, including the sample-to-detector distance. An empty capillary similar to that used for holding the NC sample was measured for the background estimation. Diffraction images were azimuthally integrated and converted into intensity profiles versus 2ϑ and versus momentum transfer, $Q = 4\pi\sin\vartheta/\lambda$, by using the FIT2D program.[13] The PDF profile was calculated up to interatomic distances r of 40 Å with a step of 0.005 Å from the Q profile by the program PDFGetX3.[14] The s maximum value of Q for the PDF calculation was set to 23.3 $Å^{-1}$ to prevent large termination effects while preserving the signal-to-noise ratio.

The program RootProf[15,16] was used to convert the XPD profiles in the CuKα_1 wavelength; EXPO2014[17] was applied for the *ab initio* structure solution from XPD data; PDFGUI[18] and FullProf[19] were used for structure refinement in direct and reciprocal space, respectively; and *VESTA*[20] and *EXPO2014* were applied for molecular graphics, *publCIF*[21] for preparing the published material.

Optical Characterization. The optical properties of the $AgBiSCl_2$ NCs were investigated on both colloidal dispersions and thin films.

A PerkinElmer UV/vis/NIR spectrophotometer (Lambda 1050) was used to measure the transmission spectra of the NCs in the 300−1600 nm range.

The photoinduced luminescence (PL) was acquired on a custom-made setup equipped with an objective (10×; Olympus, N.A. = 0.3) for reflection measurements. The samples, prepared by drop casting a toluene NC dispersion on Si substrates, were excited with a pulsed ∼50 fs laser at a 10 kHz repetition rate (Coherent, Legend) through the objective. The 800 nm output signal was frequency doubled by using a BBO crystal (Thorlabs, β-BaB_2O_4, NLC01), thus generating the 400 nm laser beam that excited the samples. After the BBO crystal, a band-pass filter (Thorlabs, FBH400-10) was used to remove the residual of the 800 nm pumping beam. The detected signal was collected by the same objective and focused, by using a 50 cm lens, into a 300 mm spectrometer (Princeton Instruments, Acton Spectra Pro SP-2300) coupled to a charge coupled device (Princeton Instruments, Pixis

https://doi.org/10.1021/acs.chemmater.3c01403
Chem. Mater. 2023, 35, 9900−9906

400). The spectrometer used a 150 g/mm grating blazed at 600 nm. A 450 nm cutoff filter (Thorlabs-FEL0450) was placed along the detection line to cut the residual excitation laser intensity. The sample was mounted inside a nitrogen cryostat (Oxford Instruments) in order to perform temperature dependent PL measurements, whereas fluence dependent PL data were obtained by means of a continuously variable neutral density filter wheel (Thorlabs) on the excitation path. A broad band white light source (Oceanhood, ASB-XE-175) was employed for real space imaging.

Ultraviolet photoelectron spectroscopy (UPS) was used to determine the Fermi and valence band energies of the NC solids. UPS spectra were recorded by using the same spectrometer as per the XPS characterization. A He I (21.22 eV) discharge lamp was used as the photon source; spectra were acquired on an area of 55 μm in diameter at a pass energy of 10 eV and with a dwell time of 100 ms.

First Principles Simulations. Density functional theory (DFT) simulations were run to infer the electronic band structure of the $AgBiSCl_2$ NCs. The calculations were run through the VASP code[22] within the plane augmented wave framework.[23] When not otherwise specified, the HSE functional[24] was adopted, and the spin−orbit coupling (SOC) was explicitly included. The plane-wave energy cutoff was set to 400 eV and the reciprocal space was sampled through a uniform, Γ-centered grid with $0.28/2\pi$ Å^{-1} point spacing. The cell parameters and atomic positions were kept frozen for the experimental estimate. The self-consistent procedures were stopped when the energy difference between two consecutive steps was lower than 10^{-7} eV. Structures and isosurfaces were drawn with the VESTA software.[20]

RESULTS AND DISCUSSION

Our synthetic protocol involved the hot-co-injection of both the S and Cl precursors ($(Me_3Si)_2S$ and BzCl, respectively) to a solution containing previously prepared Ag-thiolate and Bi-carboxylate complexes (details are given in the Experimental Section). This strategy allows tuning the Ag:Bi:S:Cl stoichiometric ratio by independently controlling the precursor concentrations and to directly access the chosen reaction temperature (130 °C, in this case). This approach also prevents the use of ligands that may act as reductants such as the commonly employed oleylamine, thus inhibiting the eventual formation of metallic Ag and Bi. Upon the coinjection of both the anion precursors, a dispersion formed, which turned to an orangish color after few minutes (Figure 1a; additional details are given in the Experimental Section). A BF-TEM inspection of the reaction product revealed rather uniform elongated NCs (Figure 1b).

The crystal structure of the as-synthesized NCs, determined *ab initio* by EXPO2014 (see Supporting Information), was validated and further refined by pair distribution function (PDF) and X-ray powder diffraction (XPD) profile fitting with the software PDFGUI and FullProf, respectively (Figure 2a,b; the main refinement results are listed in Tables S1 and S2). The refined model matched well the orthorhombic *Cmcm* structure reported for $AgBiSCl_2$ (POW_COD no. 00-150-9232, ICSD no. 413290).[10] Such a structure can be described by alternated slabs of $[AgS_2Cl_4]^{7-}$ distorted octahedra and $[BiS_2Cl_6]^{7-}$ biaugmented triangular prisms, resulting in a layered structure with stacking direction parallel to the *b* crystallographic axis (Figure 2c; refined fractional atomic coordinates, isotropic displacement parameters, and geometric parameters are listed in Table S3). These alternate Ag and Bi slabs, which display no separation, make $AgBiSCl_2$ a member of the pavonite homologue series with $n = 0$.[25]

The refined lattice parameters of our nanocrystals displayed a slight anisotropic contraction when compared to those

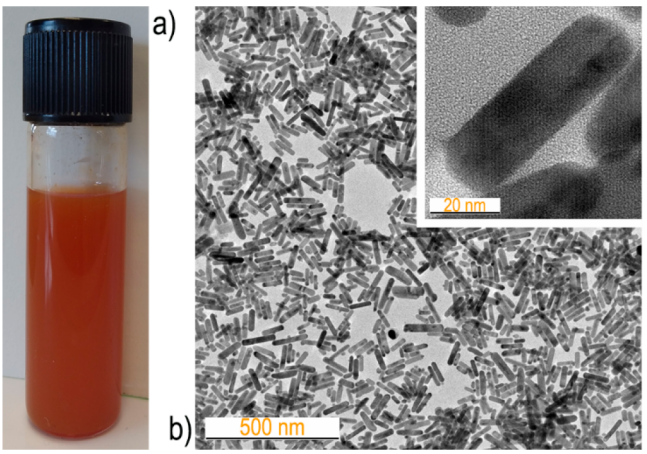

Figure 1. (a) Daylight picture of a toluene dispersion of $AgBiSCl_2$ NCs. (b) TEM micrograph of the as-synthesized colloidal $AgBiSCl_2$ NCs (the inset shows a higher magnification view).

reported for the published $AgBiSCl_2$ (a = 3.954 Å → a_p = 3.971 Å, $\Delta a/a_p = -0.43\%$; b = 13.550 Å → b_p = 13.712 Å, $\Delta b/b_p = -1.18\%$; c = 8.791 Å → c_p = 8.824 Å, $\Delta c/c_p = -0.37\%$), with the most affected crystallographic direction being that of the stacking layers (the *b* axis; Figure 2c). An analogous anisotropic contraction was observed for the cell parameters refined from PDF data (a = 3.944 Å → a_p = 3.971 Å, $\Delta a/a_p = -0.68\%$; b = 13.524 Å → b_p = 13.712 Å, $\Delta b/b_p = -1.37\%$; c = 8.775 Å → c_p = 8.824 Å, $\Delta c/c_p = -0.55\%$). The two final structure models based on independent refinement processes, working on direct (PDF) and reciprocal (XPD) space, were strongly overlaid (RMSD = 0.039 Å), assessing the reliability of our structural analysis.

The Rietveld analysis of XPD data, performed with FullProf and including anisotropic factors accounting for the crystallite shape (Table S3 and Figure S1), indicates [100] as the direction of maximal length, suggesting that the NCs preferentially grow along the *a* crystallographic axis (Table S2). HR-TEM analysis, in addition to accounting for a high degree of crystallinity of our colloidal $AgBiSCl_2$, confirmed the indications gathered from the structural data: the $AgBiSCl_2$ NCs tend to grow along the *a* crystallographic direction (Figure 3). This further indicates that $AgBiSCl_2$ strongly favors growth along the direction that guarantees maximal connectivity to its constituting polyhedra. Indeed, the $[AgS_2Cl_4]^{7-}$ octahedra share edges along *a*, but only vertices along *c*; likewise, the $[BiS_2Cl_6]^{7-}$ prisms share faces along *a*, but only edges along *c*.

TEM imaging suggests that the elongated $AgBiSCl_2$ NCs may be platelets. Such a suggestion may find partial confirmation by the Rietveld analysis of the XPD data yielding a thickness that is mildly but statistically significantly smaller than the width ([001] = 19 nm → [010] = 23 nm; Table S2). In addition, HAADF-STEM imaging, thanks to its thickness contrast, supports the platelet-like morphology of our $AgBiSCl_2$ NCs, although different orientations of the NCs on the substrate hinder straightforward statements on the NC transverse profile (Figure S3).

The elemental composition of the as-synthesized $AgBiSCl_2$ NCs was obtained by high resolution XPS analysis, which yielded a Ag:Bi:S:Cl molar ratio of 1.1:1.1:1.0:2.0 (high-resolution XPS spectra are reported in Figure S4). Our $AgBiSCl_2$ NCs thus show a metal-rich composition, in analogy

https://doi.org/10.1021/acs.chemmater.3c01403
Chem. Mater. 2023, 35, 9900−9906

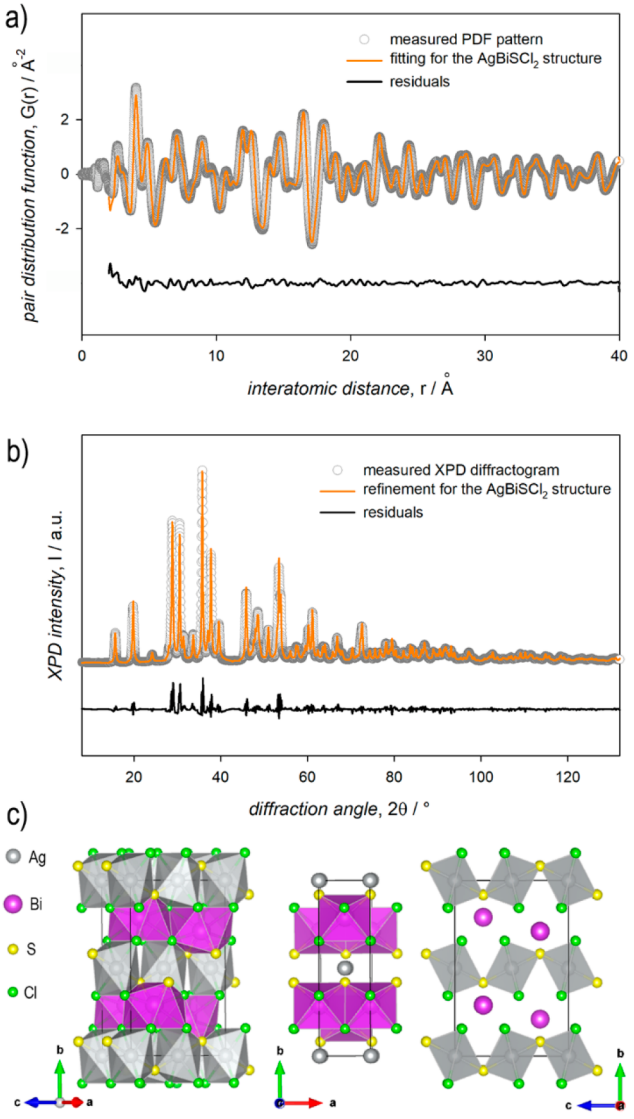

Figure 2. (a) PDF and (b) XPD profiles collected on colloidal $AgBiSCl_2$ NC powders (empty circles), with the corresponding refinement results (orange lines); residuals were offset for clarity. To facilitate the comparison with data collected on lab-grade setups, the 2θ values of the XPD horizontal axis were converted to emulate Cu $K\alpha_1$ radiation (Figure S2). (c) Model of the $AgBiSCl_2$ structure highlighting the coordination of both Ag and Bi atoms and the formation of alternate layers.

to metal chalcogenides[26] and halides[27] and to orthorhombic, ternary chalcohalides[5] that are coordinated by (metal-)oleate ligands. The homogeneous distribution of the four constituting elements at the single NC level was demonstrated by STEM-EDS compositional mapping (Figure S5).

In order to achieve an acceptably low NC polydispersity, the synthetic growth stage required time. For growth times within an hour, TEM and XPD data provided evidence of substantial morphological inhomogeneity (Figures S6) and presence of phase impurities (Figures S7); conversely, a growth time of 150 min yielded phase pure NCs with a rather low size distribution (length of 77 nm with ~25% polydispersity, width of 18 nm with ~ 20% polydispersity; Figure S8).

We also attempted to prepare sulfobromide analogues of the $AgBiSCl_2$ NCs, upon the coinjection of $(Me_3Si)_2S$ and BzBr to a hot solution of Bi-oleate and Ag-thiolate complexes.

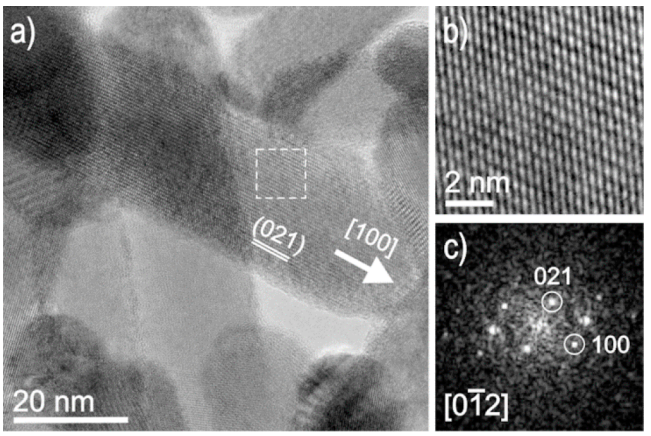

Figure 3. (a) HR-TEM image of $AgBiSCl_2$ NCs, (b) enlarged view of the region within the frame, and (c) corresponding fast Fourier transform (FFT). Identification of the orientation and directions within the NC is based on the structure identified and refined by the XPD analysis, confirming the elongation direction as the [100].

However, the resulting reaction product was constituted by a mixture of phases, including $AgBi_3S_4Br_2$, without any clear indication for the formation of the $AgBiSBr_2$ phase (Figure S9). This somehow fulfills expectations as the bulk $AgBiSX_2$ phase was only reported for X = Cl, but not for X = Br or I. We suggest that the reason may lie in the similar ionic radii of S and Cl; indeed, other studies on ternary metal sulfohalides highlighted how the reactivity and structure of the sulfochloride phases tend to be drastically different from that of the sulfobromide and sulfoiodide phases, which are instead prone to form similar structures.[5,6,28]

The absorption spectrum of a tetrachloroethylene dispersion of the colloidal $AgBiSCl_2$ NCs displayed an intense feature in the visible spectral range with a peak at ~420 nm, somewhat broadened by a slight scattering of the incident light due to the NC size and to the eventual formation of aggregates (Figure S10). The observation of an absorption peak may support the direct character of the lowest energy transition and could be used to estimate the optical band gap of the $AgBiSCl_2$ NCs (2.9 eV). UPS measurements revealed that the Fermi level of an NC film lies 1.1 eV above the valence band maximum (with a work function of 4.7 eV; Figure S11), thus slightly below the middle of the band gap. This suggests that our nanostructured $AgBiSCl_2$ may be regarded as an almost intrinsic semiconductor.

The direct character of the band gap of our NCs was corroborated by DFT calculations adopting the HSE functional, which clearly showed the lowest energy interband transition at the Y point (Figure 4), as reported for the isostructural $CuBiSCl_2$.[12] The orbital-projected density of states and charge density analyses revealed that the valence band of $AgBiSCl_2$ is formed by the S- and Cl-p orbitals and by the Ag-d orbitals, whereas the conduction band is dominated by the Bi-p orbital contribution (Figures S12 and S13).

Despite these features, no PL from $AgBiSCl_2$ NCs could be detected with a common fluorimeter in which the samples are excited by a gas-discharge lamp passing through a monochromator. We therefore investigated the $AgBiSCl_2$ NCs directly under pulsed laser excitation at relatively high fluences (10^{-2} to 10^{2} mJ/cm^2). A PL band from NCs coarsely deposited on a Si substrate was detected under a laser spot (Figure 5). White light was used to observe the real space

https://doi.org/10.1021/acs.chemmater.3c01403
Chem. Mater. 2023, 35, 9900−9906

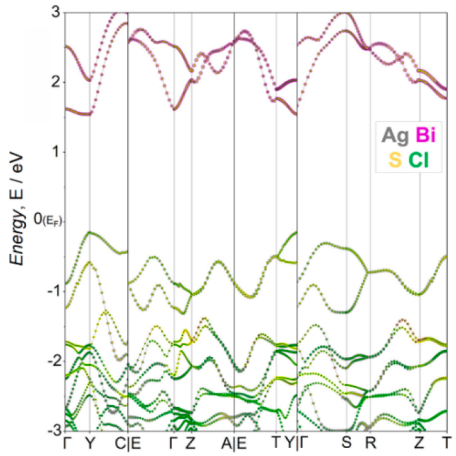

Figure 4. Calculated band structure of $AgBiSCl_2$ at the DFT/HSE level of theory; the band gap is direct and is located at the Y point.

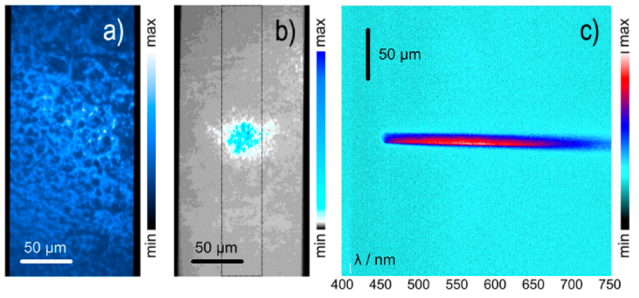

Figure 5. Real space images of (a) the $AgBiSCl_2$ NC film obtained with a white light and of (b) the laser spot on the same NC film (black side bars are the slits before the spectrometer, whereas the black thin lines in panel b account for the slit aperture in spectrally resolved PL maps). c) Spectrally resolved PL map of a $AgBiSCl_2$ NC film at room temperature upon 0.60 mJ/cm^2 pulsed excitation at 400 nm. The PL maps were used to extract the PL spectral profiles.

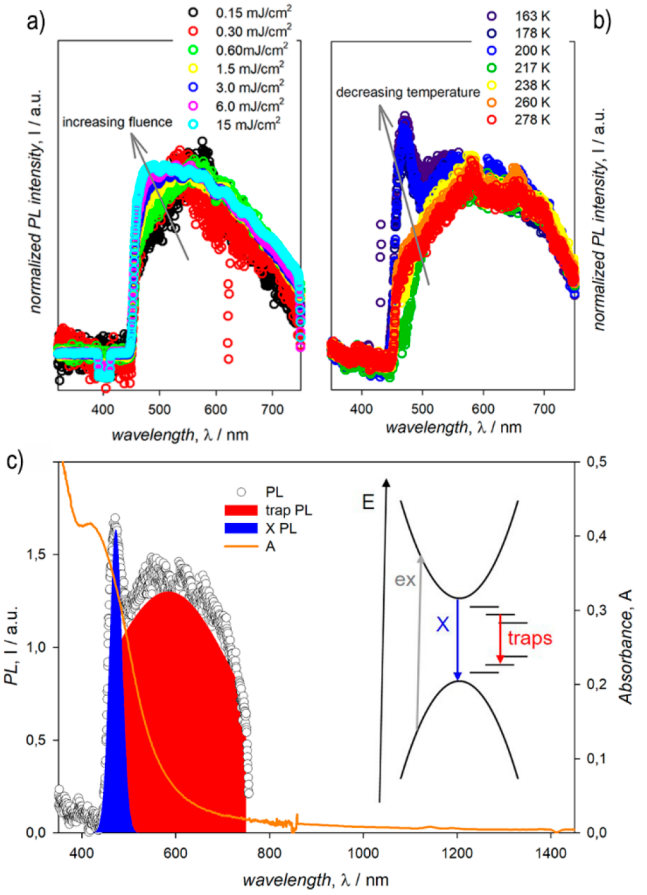

Figure 6. (a) Fluence dependent PL spectra of a $AgBiSCl_2$ NC film deposited on a Si substrate at room temperature excited at 400 nm; (b) temperature dependent PL spectra of a $AgBiSCl_2$ NC film deposited on a Si substrate at 0.60 mJ/cm^2 pulsed excitation at 400 nm; and (c) comparison of absorption and PL spectra of the colloidal $AgBiSCl_2$ NCs highlighting the band edge exciton (X) and trap state emission (a sketch of the plausible photoinduced processes is shown on the right side of the panel).

image of the NC film (Figure 5a) and the same area was excited with a laser beam (Figure 5b). The associated PL map (Figure 5c) resulted from the subtraction of both the background and substrate signals (details in Figure S14).

In order to gather information about the excited state of the $AgBiSCl_2$ NCs, we impinged an NC film with different laser fluences. In between 15 μJ/cm^2 and 15 mJ/cm^2, the integrated PL under the same spot of a NC film linearly increased (Figure S15), thus allowing for relative comparisons. The normalized PL spectra show a monotonic blue shift upon increasing excitation fluence (Figure 6a). We also investigated the effect of the temperature on the NC PL, at an intermediate fluence of 0.60 mJ/cm^2. Upon cooling the NC film, a PL peak centered at ~470 nm appeared at temperatures below 200 K (Figure 6b); unfortunately, for temperatures below 160 K, the contribution of the Si substrate prevented further evaluation of the temperature effects on the NC PL (Figure S16). On this basis, we ascribed the sharp PL peak (fwhm ~ 170 meV, estimated by Gaussian fit; highlighted in blue in Figure 6c) to the band edge emission. Indeed, this spectral feature could only be observed upon intense excitation, which likely saturates trap state emission (the broad emission band centered around 600 nm; highlighted in red in Figure 6c) allowing exciton recombination from the band edge. Analogously, lower temperatures likely inhibit the population of the trap states, again favoring the observation of band edge emission (these photoinduced processes are sketched on the right side of Figure 6c).

CONCLUSION

We successfully applied our colloidal synthetic method, based on the hot coinjection of both the chalcogen and the halogen precursors to a solution of (heavy pnictogen) metal complexes,[5,6] to the preparation of phase pure colloidal $AgBiSCl_2$ NCs. Unlike ternary Bi chalcohalides, quaternary Ag, Bi chalcohalide NCs exhibit a direct band gap, and we were able to observe the band edge PL. However, exciton recombination is dominated by nonradiative, likely trap-assisted, recombination. The identification and healing of such traps may in perspective yield an alternative blue luminophore. This could be achieved by pursuing an atomic level description of these nanocrystals and their surfaces, then improving the presented synthetic protocol and implementing postsynthesis surface chemistry modification strategies.[29] Nevertheless, this work expands the set of available heavy pnictogen chalcohalide nanomaterials and contributes to advancing the knowledge on this class of mixed anion semiconductors. More broadly, this work may stimulate

https://doi.org/10.1021/acs.chemmater.3c01403
Chem. Mater. 2023, 35, 9900−9906

collective efforts on such potentially robust, cost-effective, solution processable, and nontoxic chalcohalide nanomaterials, which may become reliable complements to the established chalcogenide and halide semiconductors.

■ ASSOCIATED CONTENT

Data Availability Statement

Crystallographic data of $AgBiSCl_2$ are deposited at the Cambridge Crystallographic Data Centre, under deposition number CSD 2260259 and can be obtained free of charge via https://www.ccdc.cam.ac.uk/structures/.

Supporting Information

The Supporting Information is available free of charge at https://pubs.acs.org/doi/10.1021/acs.chemmater.3c01403.

Synthesis; structural refinement parameters; structural and morphological characterization; electronic structure calculations; and optical properties (PDF)

Crystallographic information file for $AgBiSCl_2$ (CIF)

■ AUTHOR INFORMATION

Corresponding Authors

Anna Moliterni − *Consiglio Nazionale delle Ricerche, Istituto di Cristallografia − CNR IC, 70126 Bari, Italy;* orcid.org/0000-0001-6786-6982; Email: anna.moliterni@cnr.it

Carlo Giansante − *Consiglio Nazionale delle Ricerche, Istituto di Nanotecnologia − CNR NANOTEC, 73100 Lecce, Italy;* orcid.org/0000-0003-4558-5367; Email: carlo.giansante@nanotec.cnr.it

Authors

Danila Quarta − *Consiglio Nazionale delle Ricerche, Istituto di Nanotecnologia − CNR NANOTEC, 73100 Lecce, Italy*

Stefano Toso − *Istituto Italiano di Tecnologia − IIT, 16163 Genova, Italy;* orcid.org/0000-0002-1621-5888

Antonio Fieramosca − *Consiglio Nazionale delle Ricerche, Istituto di Nanotecnologia − CNR NANOTEC, 73100 Lecce, Italy*

Lorenzo Dominici − *Consiglio Nazionale delle Ricerche, Istituto di Nanotecnologia − CNR NANOTEC, 73100 Lecce, Italy*

Rocco Caliandro − *Consiglio Nazionale delle Ricerche, Istituto di Cristallografia − CNR IC, 70126 Bari, Italy;* orcid.org/0000-0002-0368-4925

David Maria Tobaldi − *Consiglio Nazionale delle Ricerche, Istituto di Nanotecnologia − CNR NANOTEC, 73100 Lecce, Italy*

Gabriele Saleh − *Istituto Italiano di Tecnologia − IIT, 16163 Genova, Italy;* orcid.org/0000-0002-6201-9546

Irina Gushchina − *Istituto Italiano di Tecnologia − IIT, 16163 Genova, Italy; Department of Chemistry and Biochemistry, University of Notre Dame, Notre Dame, Indiana 46556, United States*

Rosaria Brescia − *Istituto Italiano di Tecnologia − IIT, 16163 Genova, Italy;* orcid.org/0000-0003-0607-0627

Mirko Prato − *Istituto Italiano di Tecnologia − IIT, 16163 Genova, Italy;* orcid.org/0000-0002-2188-8059

Ivan Infante − *Istituto Italiano di Tecnologia − IIT, 16163 Genova, Italy; BCMaterials, Basque Center for Materials, Applications, and Nanostructures, Leioa 48940, Spain; Ikerbasque, Basque Foundation for Science, Bilbao 48009, Spain;* orcid.org/0000-0003-3467-9376

Adriano Cola − *Consiglio Nazionale delle Ricerche, Istituto di Microelettronica e Microsistemi − CNR IMM, 73100 Lecce, Italy*

Cinzia Giannini − *Consiglio Nazionale delle Ricerche, Istituto di Cristallografia − CNR IC, 70126 Bari, Italy;* orcid.org/0000-0003-0983-2885

Liberato Manna − *Istituto Italiano di Tecnologia − IIT, 16163 Genova, Italy;* orcid.org/0000-0003-4386-7985

Giuseppe Gigli − *Consiglio Nazionale delle Ricerche, Istituto di Nanotecnologia − CNR NANOTEC, 73100 Lecce, Italy; Dipartimento di Fisica, Università del Salento, 73100 Lecce, Italy*

Complete contact information is available at: https://pubs.acs.org/10.1021/acs.chemmater.3c01403

Author Contributions

†D.Q. and S.T. contributed equally. All authors have given approval to the final version of the manuscript.

Funding

S.T., G.S., and L.M. acknowledge funding from the programme MiSE-ENEA under the Grant "Italian Energy Materials Acceleration Platform − IEMAP".

Notes

The authors declare the following competing financial interest(s): C. Gians., D.Q., S.T., R.C., A.M., C. Giann., L.M., and G.G. are co-inventors on a provisional patent application entitled Process for the Production of Nanocrystals of Metal Chalcohalides, PCT/IB2023/050820.

■ ACKNOWLEDGMENTS

The access to the National Synchrotron Light Source, Brookhaven National Laboratory, was supported by the U.S. Department of Energy, Office of Science, Office of Basic Energy Sciences, under Contract No. DE-AC02-98CH10886 (NSLS-II Proposal Number 307441). The computing resources and the related technical support used for this work have been provided by CRESCO/ENEAGRID High Performance Computing infrastructure and its staff.[30] CRESCO/ENEAGRID High Performance Computing infrastructure is funded by ENEA, the Italian National Agency for New Technologies, Energy and Sustainable Economic Development and by Italian and European research programs, see http://www.cresco.enea.it/english for information. R.C., A.M., and C. Giann. gratefully thank B.M. Aresta and G. Filograsso for their administrative support.

■ REFERENCES

(1) Wlaźlak, E.; Blachecki, E.; Bisztyga-Szklarz; Klejna, S.; Mazur, T.; Mech, K; Pilarczyk, K; Przyczyna, D; Suchecki, M; Zawal, P; Szaciłowski, K. Heavy pnictogen chalcohalides: the synthesis, structure and properties of these rediscovered semiconductors. *Chem. Commun.* **2018**, *54*, 12133−12162.

(2) Ghorpade, U V.; Suryawanshi, M P.; Green, M. A.; Wu, T; Hao, X.; Ryan, K. M. Emerging Chalcohalide Materials for Energy Applications. *Chem. Rev.* **2023**, *123*, 327−378.

(3) Palazon, F. Metal Chalcohalides: Next Generation Photovoltaic Materials? *Solar RRL* **2022**, *6*, 2100829.

(4) Choi, Y. C.; Nie, R. Heavy pnictogen chalcohalides for efficient, stable, and environmentally friendly solar cell applications. *Nanotechnology* **2023**, *34*, 142001.

(5) Quarta, D.; Toso, S.; Giannuzzi, R.; Caliandro, R.; Moliterni, A.; Saleh, G.; Capodilupo, A.-L.; Debellis, D.; Prato, M.; Nobile, C.; Maiorano, V.; Infante, I.; Gigli, G.; Giannini, C.; Manna, L.;

Giansante, C. Colloidal Bismuth Chalcohalide Nanocrystals. *Angew. Chem., Int. Ed.* **2022**, *61*, No. e202201747.
(6) Quarta, D.; Toso, S.; Saleh, G.; Caliandro, R.; Moliterni, A.; Griesi, A.; Divitini, G.; Infante, I.; Gigli, G.; Giannini, C.; Manna, L.; Giansante, C. Mixed Valence of Bismuth in Hexagonal Chalcohalide Nanocrystals. *Chem. Mater.* **2023**, *35*, 1029.
(7) Kangsabanik, J.; Svendsen, M. K.; Taghizadeh, A.; Crovetto, A.; Thygesen, K. S. Indirect Band Gap Semiconductors for Thin-Film Photovoltaics: High-Throughput Calculation of Phonon-Assisted Absorption. *J. Am. Chem. Soc.* **2022**, *144*, 19872.
(8) Islam, S. M.; Malliakas, C. D.; Sarma, D.; Maloney, D. C.; Stoumpos, C. C.; Kontsevoi, O. Y.; Freeman, A. J.; Kanatzidis, M. G. Direct Gap Semiconductors $Pb_2BiS_2I_3$, $Sn_2BiS_2I_3$, and Sn_2BiSI_5. *Chem. Mater.* **2016**, *28*, 7332.
(9) Roth, A. N.; Opare-Addo, J.; Gi, E.; Mena, S.; Guirado, G.; Schaller, R. D.; Smith, E. A.; Vela, J. Solution-Phase Synthesis and Photoluminescence of Quaternary Chalcohalide Semiconductors. *Chem. Mater.* **2023**, *35*, 2165.
(10) Ruck, M.; Poudeu Poudeu, P. F.; Söhnel, T. Synthesis, Crystal Structure and Electronic Band Structure of the Isostructural Sulfide Chlorides $CuBiSCl_2$ and $AgBiSCl_2$. *Z. Anorg. Allg. Chem.* **2004**, *630*, 63.
(11) Choudhary, K.; Bercx, M.; Jiang, J.; Pachter, R.; Lamoen, D.; Tavazza, F. Accelerated Discovery of Efficient Solar Cell Materials Using Quantum and Machine-Learning Methods. *Chem. Mater.* **2019**, *31*, 5900.
(12) Ming, C.; Chen, Z.; Zhang, F.; Gong, S.; Wu, X.; Jiang, J.; Ye, T.; Xu, Q.; Yang, K.; Wang, L.; Cao, X.; Yang, S.; Zhang, S.; Zhang, Y.; Shi, J.; Sun, Y.-Y. Mixed Chalcogenide-Halides for Stable, Lead-Free and Defect-Tolerant Photovoltaics: Computational Screening and Experimental Validation of $CuBiSCl_2$ with Ideal Band Gap. *Adv. Funct. Mater.* **2022**, *32*, 2112682.
(13) Hammersley, A. P.; Svensson, S. O.; Hanfland, M.; Fitch, A. N.; Hausermann, D. Two-dimensional detector software: From real detector to idealised image or two-theta scan. *High Press. Res.* **1996**, *14*, 235.
(14) Juhás, P.; Davis, T.; Farrow, C. L.; Billinge, S. J. L. PDFgetX3: a rapid and highly automatable program for processing powder diffraction data into total scattering pair distribution functions. *J. Appl. Crystallogr.* **2013**, *46*, 560.
(15) Caliandro, R.; Belviso, B. D. RootProf: software for multivariate analysis of unidimensional profiles. *J. Appl. Crystallogr.* **2014**, *47*, 1087.
(16) Mazzone, A.; Lopresti, M.; Belviso, B. D.; Caliandro, R. New features of the RootProf program for model-free analysis of unidimensional profiles. *J. Appl. Crystallogr.* **2023**, DOI: 10.1107/S1600576723008348.
(17) Altomare, A.; Cuocci, C.; Giacovazzo, C.; Moliterni, A.; Rizzi, R.; Corriero, N.; Falcicchio, A. EXPO2013: A kit of tools for phasing crystal structures from powder data. *J. Appl. Crystallogr.* **2013**, *46*, 1231.
(18) Farrow, C. L.; Juhás, P.; Liu, J. W.; Bryndin, D.; Božin, E. S.; Bloch, J.; Proffen, T.; Billinge, S. J. L. PDFfit2 and PDFgui: computer programs for studying nanostructure in crystals. *J. Phys.: Condens. Matter* **2007**, *19*, 335219.
(19) Rodríguez-Carvajal, J. Recent advances in magnetic structure de-termination by neutron powder diffraction. *Phys. B: Condensed Matter* **1993**, *192*, 55.
(20) Momma, K.; Izumi, F. VESTA 3 for three-dimensional visualization of crystal, volumetric and morphology data. *J. Appl. Crystallogr.* **2011**, *44*, 1272.
(21) Westrip, S. P. publCIF: Software for Editing, Validating and Formatting Crystallographic Information Files. *J. Appl. Crystallogr.* **2010**, *43*, 920.
(22) Kresse, G.; Furthmüller, J. Efficiency of ab-initio total energy calculations for metals and semiconductors using a plane-wave basis set. *Comput. Mater. Sci.* **1996**, *6*, 15.
(23) Blöchl, P. E. Projector augmented-wave method. *Phys. Rev. B* **1994**, *50*, 17953.
(24) Heyd, J.; Scuseria, G. E.; Ernzerhof, M. Hybrid functionals based on a screened Coulomb potential. *J. Chem. Phys.* **2003**, *118*, 8207.
(25) Zhao, J.; Hao, S.; Islam, S. M.; Chen, H.; Tan, G.; Ma, S.; Wolverton, C.; Kanatzidis, M. G. Six Quaternary Chalcogenides of the Pavonite Homologous Series with Ultralow Lattice Thermal Conductivity. *Chem. Mater.* **2019**, *31*, 3430.
(26) Grisorio, R.; Debellis, D.; Suranna, G. P.; Gigli, G.; Giansante, C. The Dynamic Organic/Inorganic Interface of Colloidal PbS Quantum Dots. *Angew. Chem., Int. Ed.* **2016**, *55*, 6628.
(27) Quarta, D.; Imran, M.; Capodilupo, A.-L.; Petralanda, U.; van Beek, B.; De Angelis, F.; Manna, L.; Infante, I.; De Trizio, L.; Giansante, C. Stable Ligand Coordination at the Surface of Colloidal $CsPbBr_3$ Nanocrystals. *J. Phys. Chem. Lett.* **2019**, *10*, 3715.
(28) Toso, S.; Akkerman, Q. A.; Martín-García, B.; Prato, M.; Zito, J.; Infante, I.; Dang, Z.; Moliterni, A.; Giannini, C.; Bladt, E.; Lobato, I.; Ramade, J.; Bals, S.; Buha, J.; Spirito, D.; Mugnaioli, E.; Gemmi, M.; Manna, L. Nanocrystals of Lead Chalcohalides: A Series of Kinetically Trapped Metastable Nanostructures. *J. Am. Chem. Soc.* **2020**, *142*, 10198.
(29) Giansante, C. Library Design of Ligands at the Surface of Colloidal Nanocrystals. *Acc. Chem. Res.* **2020**, *53*, 1458.
(30) Ponti, G. et al. The role of medium size facilities in the HPC ecosystem: the case of the new CRESCO4 cluster integrated in the ENEAGRID infrastructure. *Proceedings of the 2014 International Conference on High Performance Computing and Simulation, HPCS*; IEEE: 2014; accession number 6903807, p 1030.

https://doi.org/10.1021/acs.chemmater.3c01403
Chem. Mater. 2023, 35, 9900−9906